[17]W. -F. Lin, Phys. Letters 39B, 447 (1972).
[18]J. Friedrich and F. Lenz, Nucl. Phys. A183, 523 (1972).
[19]W. Bertozzi, J. Friar, J. Heisenberg, and J. W. Negele, Phys. Letters 41B, 477 (1972).

PHYSICAL REVIEW C VOLUME 7, NUMBER 5 MAY 1973

Scattering of 139-MeV Alpha Particles by ^{58}Ni and ^{208}Pb†

D. A. Goldberg, S. M. Smith, H. G. Pugh, P. G. Roos, and N. S. Wall
Department of Physics and Astronomy, University of Maryland, College Park, Maryland 20742
(Received 18 December 1972)

The elastic and inelastic scattering of α particles by ^{58}Ni and ^{208}Pb has been investigated at an incident energy of 139 MeV. The elastic cross sections have been analyzed in terms of the optical model using a six-parameter Woods-Saxon potential. The data for ^{58}Ni are sufficient to eliminate the discrete ambiguity in the strength of the potential; the single potential which fits the data has a well depth of 116 MeV and a volume integral $J/4A$ of 298 MeV fm^3. For ^{208}Pb the discrete ambiguity could not be resolved. This outcome is consistent with recently developed criteria for experimental data necessary to resolve the discrete ambiguity. A discussion of the discrete ambiguity, in particular the A dependence, is given, and it is shown that measurements at higher energies are required to resolve the ambiguity for ^{208}Pb. The inelastic cross sections for transitions to the 1.45-MeV ($J^\pi = 2^+$), 2.46-MeV (4^+), 4.47-MeV (3^-) states in ^{58}Ni and the 2.62-MeV (3^-) state in ^{208}Pb have been analyzed with distorted-wave Born-approximation (DWBA) calculations using collective-model form factors. The results are consistent with previous analyses of lower-energy data.

I. INTRODUCTION

Although the study of α-particle scattering has a long history, only recently have such investigations been performed at energies above 100 MeV. Several systematic studies have now been made at 104[1] and 166 MeV.[2] We have extended these investigations by examining the elastic and inelastic scattering of α particles by ^{58}Ni and ^{208}Pb at 139 MeV.

Elastic scattering data are conventionally analyzed in terms of the optical model. Since such analyses provide a convenient avenue for obtaining scattering wave functions, the extraction of optical potentials from elastic scattering data is generally the first step in extracting nuclear structure information from other reactions involving an elastic α channel. Unfortunately, the ability to extract such information, for example, spectroscopic strengths from (^{3}He, α) reactions,[3] has been somewhat hampered at lower energies by the well-known ambiguities[4] in the α optical potential parameters. Investigations seeking information directly from the elastic scattering results, such as those attempting to determine nuclear matter distributions directly from comparisons between phenomenological and microscopic α optical potentials,[5] have likewise been hampered.

Some evidence that one might be able to resolve the discrete ambiguities using higher incident energies appears in the studies referred to above.[1,2] In addition an analysis by Duhm[6] of the elastic scattering of 119-MeV α particles by ^{24}Mg indicates no discrete ambiguity. It was therefore felt that additional investigations at higher energies might yield unambiguous results, and therefore provide information on the systematics of intermediate energy elastic scattering. It was also hoped that such investigations might lead to a better understanding of the discrete ambiguity and perhaps the means for removing it as well. The present work contains the results of the first part of that investigation.

As a result of a preliminary analysis of the present elastic data,[7] two of the present authors have developed an interpretation of the elastic scattering of composite projectiles at intermediate energies[8] which emphasizes the refractive aspects of the process rather than the more commonly discussed diffractive aspects; they also outlined criteria for the incident energy and angular range of measurements required to eliminate the discrete ambiguities in the optical potentials for such projectiles.[9] The criteria are reviewed here briefly, and the elastic scattering data which led to their formulation are discussed is some detail. In Sec. III B the size or A dependence of the required incident energy is demonstrated through a comparison of the ^{58}Ni and ^{208}Pb elastic scattering results. Also, by examining the effective optical potentials (nuclear plus Coulomb plus centrifugal), we are able to demonstrate explicitly why the phase-

shift equivalence of the potentials comprising the discrete ambiguity[4] ceases to exist at higher incident energies.

In Sec. IV the inelastic transitions to the low-lying states of ^{58}Ni and ^{208}Pb are discussed. The scattering wave functions from the optical-model analyses were employed in distorted-wave Born-approximation (DWBA) calculations with collective-model form factors to extract transition strengths. The results are compared with those obtained from studies at lower energies and are also examined to determine if the ability to extract an unambiguous optical potential affects the extracted strengths.

II. EXPERIMENTAL PROCEDURE

The α particles were accelerated to an energy of 139 MeV by the University of Maryland isochronous cyclotron and directed through the beam handling system shown in Fig. 1. The beam transport system was operated in a dispersive mode: The beam passing through slits S2 was focused at slits S5; the energy-analyzed beam was then focused at the center of the 1.5-m diameter precision scattering chamber where the experimental measurements were performed. Within the chamber the scattered particles were detected by two cooled 4-mm lithium-drifted silicon counters mounted on separate movable arms, positioned by remotely controlled digital stepping motors. One of the detectors was employed as an additional beam monitor to accompany the Faraday cup system. The counters were oriented at 60° relative to the respective axes of the arms to provide an effective stopping thickness of 8 mm.

For forward-angle measurements a rectangular detector aperture of nominally $\frac{1}{4}$° horizontally by 1° vertically was employed, whereas for the large-angle regions where the cross sections did not vary rapidly the measurements were performed with an opening of nominally 1° horizontally by 2° vertically. The relative error in the angular positioning of the detector arms was at most ±0.02° (lab).

The amplified signals from the detectors were analyzed in two separate 8192 channel Nuclear Data Inc. analog-to-digital conversion (ADC) units. On-line data analysis of the energy spectra was

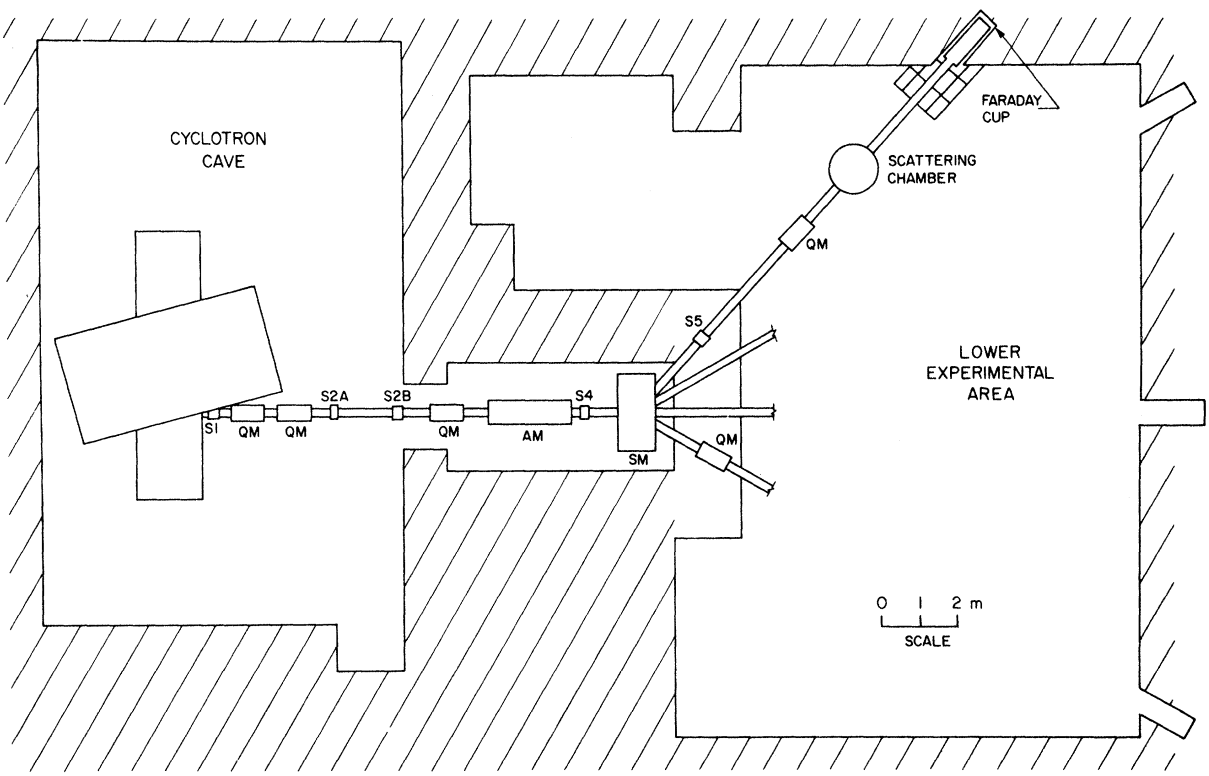

FIG. 1. Beam transport system to lower experimental area of the University of Maryland Cyclotron Laboratory. The units labeled QM are doublet quadrupole magnets, S1 through S5 are horizontal and vertical slits systems, SM is the analyzing and switching magnet, and AM is an analyzing and bending magnet for transporting the beam to the upper experimental area (not shown).

performed using an IBM 360/44 computer.

The beam energy and its angular offset about the geometrical zero of the scattering chamber were determined by a kinematic method which differs from the conventional crossover technique.[10] This latter method is unsuitable at high incident α energies because the crossover angle typically varies less than the relative angular error for incident energy variations of a few MeV. In the present investigation we employed a least-squares analysis to obtain the incident beam energy, the offset angle of the beam, the α-particle energy per ADC channel, and the zero-energy channel in the ADC unit, from the measured ADC channel positions of several spectrum peaks at several scattering angles. The channel positions of the peaks used were those resulting from the following reactions on a thin CH target: $^{12}C(\alpha, \alpha)^{12}C$, $^{1}H(\alpha, \alpha)^{1}H$, and $^{1}H(\alpha, {}^{3}He)^{2}H$. The *relative* peak positions from the latter two reactions on ^{1}H are fairly sensitive to variations in the incident energy and beam position. The accuracy of this method is limited by the accuracy in the determination of the mean position and energy of these peaks; this is primarily determined by the finite angular aperture of the detectors and the rapid energy variation of these peaks with scattering angle. In the present experiment the incident energy was determined to be 139.0 ± 0.5 MeV; the angular position of the beam was determined to within an error of $\pm 0.05°$ (lab).

The targets employed were self-supporting foils of material isotopically enriched to 99% purity. Their thicknesses were previously determined to be 2.09 ± 0.2 mg/cm^2 for ^{208}Pb and 1.60 ± 0.3 mg/cm^2 for the ^{58}Ni target.[11] Typical spectra obtained for each target are shown in Figs. 2 and 3. The average energy resolution was 200 keV full width at half maximum (FWHM).

Differential cross sections were extracted for the peaks indicated by crosshatching in Figs. 2 and 3. The elastic differential cross sections relative to Rutherford cross sections are displayed in Figs. 4 and 5. Relative cross sections for each peak were obtained by normalizing the yield at each angle to the yield for the ground-state peak in the monitor detector spectrum. These relative cross sections were additionally corrected for electronic dead time in the α and monitor counter systems. This correction never exceeded 10%. The normalization factors required to express the cross sections in units of mb/sr were conventionally calculated from the detector angular acceptance, the target thickness, and the average value of the ratio of the monitor ground-state yield to the charge collected in the Faraday cup system. No corrections to the absolute cross sections were performed to account for possible count losses in a spectrum peak due to reactions within the detector. (These losses are probably[12] less than 5%.) Errors in the absolute cross-sec-

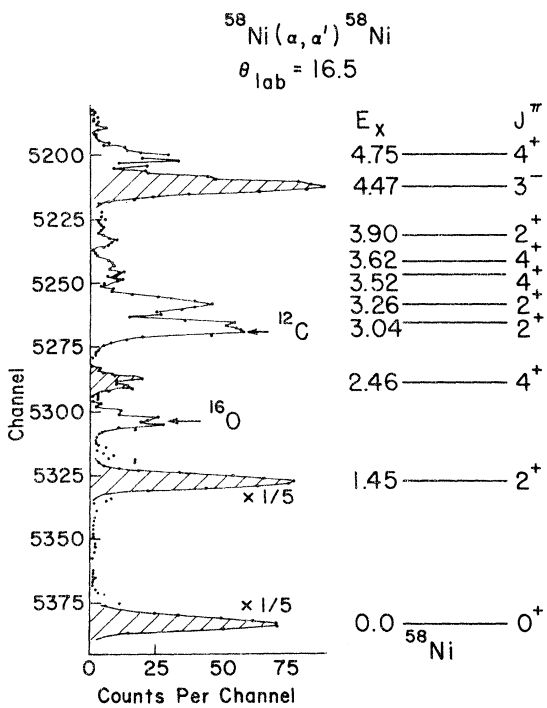

FIG. 2. The ^{58}Ni α-particle spectrum at $\theta_{lab} = 16.5°$. Differential cross sections were extracted for the peaks indicated by crosshatching.

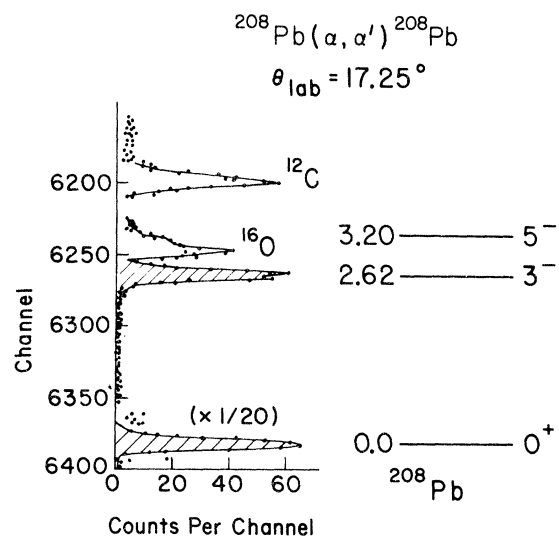

FIG. 3. The ^{208}Pb α-particle spectrum at $\theta_{lab} = 17.25°$. Differential cross sections were extracted for the peaks indicated by cross hatching.

tion normalization were estimated to be due primarily to the uncertainties in the target thicknesses previously specified.

The relative errors displayed in Figs. 4 and 5 are primarily based on statistical errors in the determinations of a peak's area and background level. However, all data points were assigned a minimum error of 3% to account for variations from run to run in the relative normalizations obtained from the two separate beam monitor systems. Relative errors were increased to reflect the effects of uncertainties in the zero angle. The magnitudes of these errors were estimated from the variation of the cross section with angle.

III. OPTICAL-MODEL ANALYSIS

A. Procedure and Results

The elastic scattering data were analyzed conventionally using the optical-model code[13] JIB3 (modified to permit the use of up to 100 partial waves). We employed a six-parameter Woods-Saxon optical potential of the form

$$U(r) = -Vf(x) - iWf(x') + V_c(r), \quad (1)$$

where $f(x) = (1+e^x)^{-1}$, $x = (r - r_0A^{1/3})/a$, $x' = (r - r_0'A^{1/3})/a'$, and V_c is the electrostatic potential of a uniformly charged sphere. The parameters were determined by fitting the data to minimize the quantity

$$\chi^2 = \sum_{i=1}^{n} \{[\sigma_{\rm th}(\theta_i) - \sigma_{\rm exp}(\theta_i)]/\Delta\sigma(\theta_i)\}^2 . \quad (2)$$

The determination of the relative errors $\Delta\sigma(\theta_i)$ was described in Sec. II.

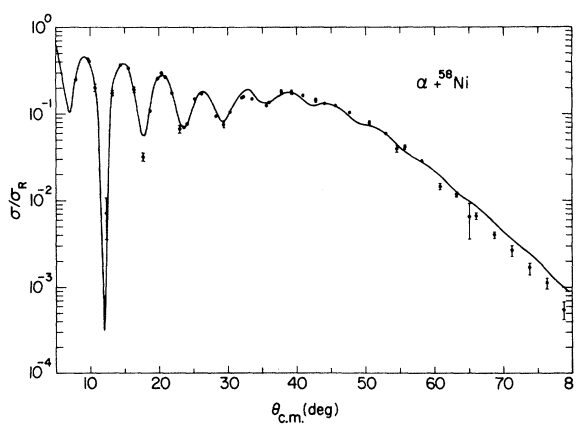

FIG. 4. ^{58}Ni elastic differential cross section as a ratio to Rutherford scattering. The curve is an optical-model fit to the data obtained with the parameter set given in Table I. The error bars include the effects of uncertainty in the zero angle (see text).

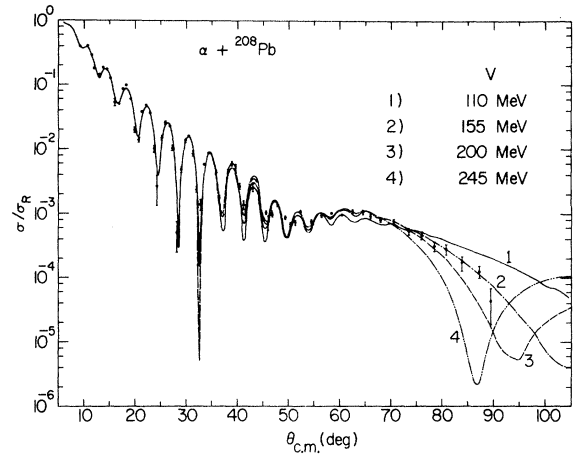

FIG. 5. ^{208}Pb elastic differential cross section as a ratio to Rutherford scattering. The various curves are optical-model fits to the data obtained with the parameter sets given in Table I. The error bars include the effects of uncertainty in the zero angle (see text).

For both nuclei a systematic grid search was performed by fixing V at a number of different values and then allowing the remaining five parameters to vary in order to minimize χ^2. The values of V employed ranged from 55 to 270 MeV. In order to insure that at each value of V the minimum χ^2 was determined for reasonable starting

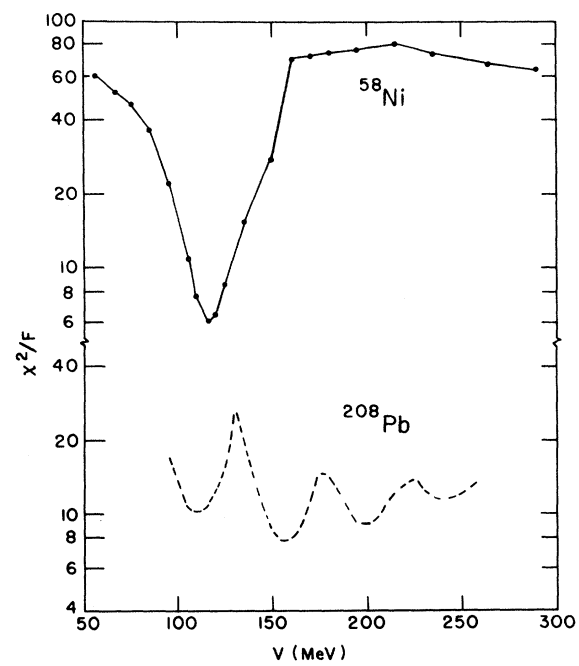

FIG. 6. Values of χ^2/F for ^{58}Ni and ^{208}Pb obtained from attempts to fit the data with different values of the real well depth V.

TABLE I. Optical-potential parameters. The form of the optical potential employed is given in the text. To this potential was added the potential of a uniformly charged sphere of radius $R_c = r_c A^{1/3}$. The last two columns list the χ^2 values per degree of freedom for the fits to the data, and the volume integral per target-projectile nucleon pair for the real part of the potential.

Target	V (MeV)	r (fm)	a (fm)	W (MeV)	r' (fm)	a' (fm)	r_c (fm)	χ^2/F	$J/4A$ (MeV fm^3)
^{58}Ni	116.4	1.245	0.793	20.52	1.595	0.571	1.40	6.2	298
^{208}Pb 1	110.0	1.315	0.705	21.27	1.509	0.673	1.40	10.0	283
2	155.0	1.282	0.677	23.26	1.478	0.733	1.40	7.6	369
3	200.0	1.261	0.657	24.50	1.462	0.767	1.40	9.1	452
4	245.0	1.245	0.647	25.89	1.448	0.788	1.40	11.3	532

values of the remaining parameters, the variation of the final parameter values with V was examined for abrupt changes[14]; additional searches were performed at the same value of V but at different starting values of the other parameters when such irregularities appeared.

The results of the searches are presented in Fig. 6. In the case of ^{58}Ni, V was also allowed to vary to determine the final parameter values which minimized χ^2; for ^{208}Pb the minima in χ^2 were sufficiently broad that six-parameter seaches were not deemed useful. The parameter values corresponding to the minima are summarized in Table I; the differential cross sections calculated from these potentials are displayed with the data in Figs. 4 and 5.

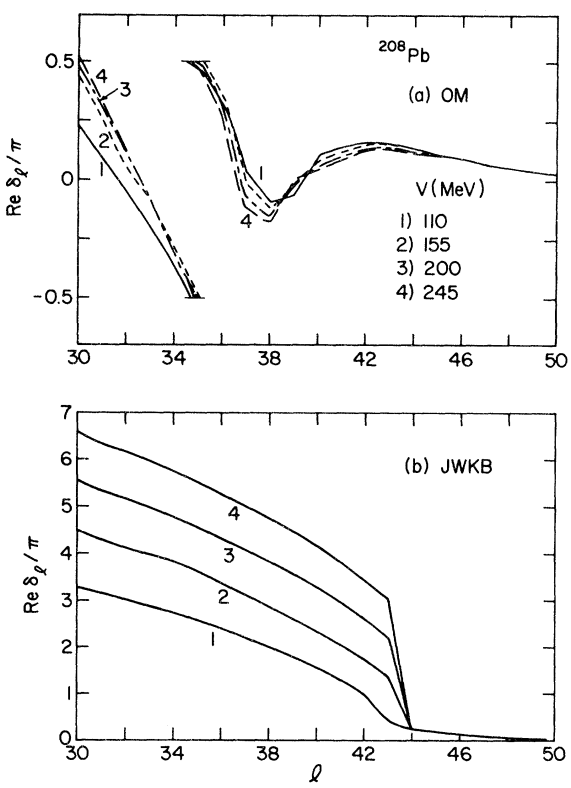

FIG. 7. Real nuclear phase shifts obtained from fitting the ^{208}Pb elastic cross sections: (a) exact optical-model (OM) results using the ^{208}Pb potentials of Table I; (b) results obtained from the JWKB calculations for the same potentials.

The appearance of multiple minima in the graphs of χ^2 vs V is commonly referred to as the discrete ambiguity[4] in optical potentials. It has been pointed out previously[15] that potentials in the neighborhood of a given minimum in χ^2 are all characterized by an approximately constant volume integral despite what may be fairly wide variations in V. Such potentials, having essentially the same volume integral, are described as belonging to a single "family" of potentials.[16] The relatively slow variation of χ^2 with V near the χ^2 minimum within a given family is frequently referred to as the continuous ambiguity.

For ^{58}Ni only a single over-all minimum was obtained, i.e., only a single family was found. This family is characterized by a well depth of 116.4 MeV and a volume integral per target-projectile nucleon pair of about 300 MeV fm^3. In contrast, for the ^{208}Pb data a number of different families were obtained which yielded comparable minimum values of χ^2. Also, the relative depths of the minima in the χ^2 vs V curve for ^{208}Pb were significantly shallower than the depth of the single minimum in the ^{58}Ni curve.

B. *A* Dependence of the Discrete Ambiguity

The results for ^{208}Pb clearly exhibit the discrete ambiguity while those for ^{58}Ni do not. In a recent paper[9] by two of the present authors, criteria were developed for the measurements which are required to eliminate such ambiguities in the optical potentials of composite projectiles. In fact, the studies leading to the development of these criteria

employed the present ^{58}Ni data. The criteria are based on a semiclassical description of the scattering process, and are twofold. First, the incident energy must be high enough that the semiclassically defined maximum deflection angle Θ be less than 180°; this condition will manifest itself in an almost exponential falloff of the elastic cross section starting at an angle somewhat less than Θ. Secondly, the experimental data must extend into the falloff region beyond Θ. It has been shown[9] that the present ^{58}Ni data, which lead to an unambiguous determination of the optical-model parameters, satisfy the above criteria. (The value of Θ, calculated using the potential for ^{58}Ni given in Table I, is approximately 63°, and the experimental data extend to 80°.)

In Ref. 9, some simple arguments were advanced regarding the effect of nuclear size on the energy and angular range of data required to eliminate discrete ambiguities; in particular it was argued that the required incident energy increases with nuclear size. In this section we will examine this question in greater detail, and from a somewhat different perspective, by considering the origin of the phase-shift equivalence of the potentials comprising the discrete ambiguity.

It has been known for some time[4] that the discrete ambiguity arises because different potentials are able to give rise to phase shifts which are equivalent, *modulo* π; for this reason the discrete ambiguity is sometimes referred to as the phase ambiguity. To obtain a better understanding of the conditions necessary for the above equivalence, and in particular to see how its occurrence depends on bombarding energy, we consider the nuclear phase shifts corresponding to each of the ^{208}Pb potentials given in Table I which comprise the discrete ambiguity. Since the phase shifts obtained from our optical-model codes are only known *modulo* π, we performed zero-order JWKB calculations (see e.g., Ref. 9) to obtain the approximate absolute values of the phase shifts. The phase shifts obtained from the conventional optical-model calculations (*modulo* π) and the JWKB results are shown in Fig. 7. [Subtraction of the appropriate value of $n\pi$ from the phase shifts shown in Fig. 7(b) gives phase shifts approximately equal to those shown in Fig. 7(a).] The real phase shifts for a given l exhibit the $n\pi$ ($n=0,1,2,\ldots$) ambiguity characteristic of the discrete or "phase" ambiguity. In this case there is an abrupt increase in the phase shifts at $l=43$. For l values less than 43 the phase shifts for each successive family differ by

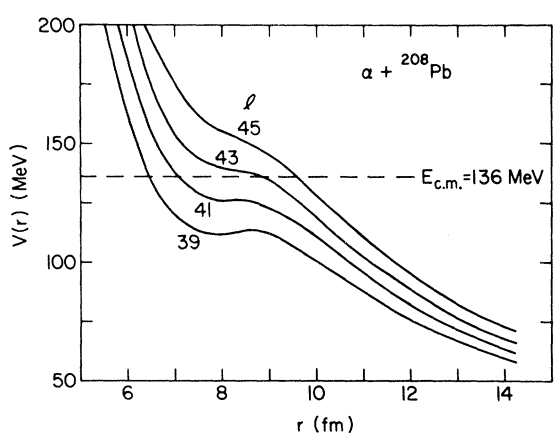

FIG. 8. ^{208}Pb effective potentials for partial waves in the vicinity of $l=43$. The energy $E_{c.m.}=136$ MeV corresponds to an incident energy of 139 MeV (lab). Potential 1 of Table I was employed.

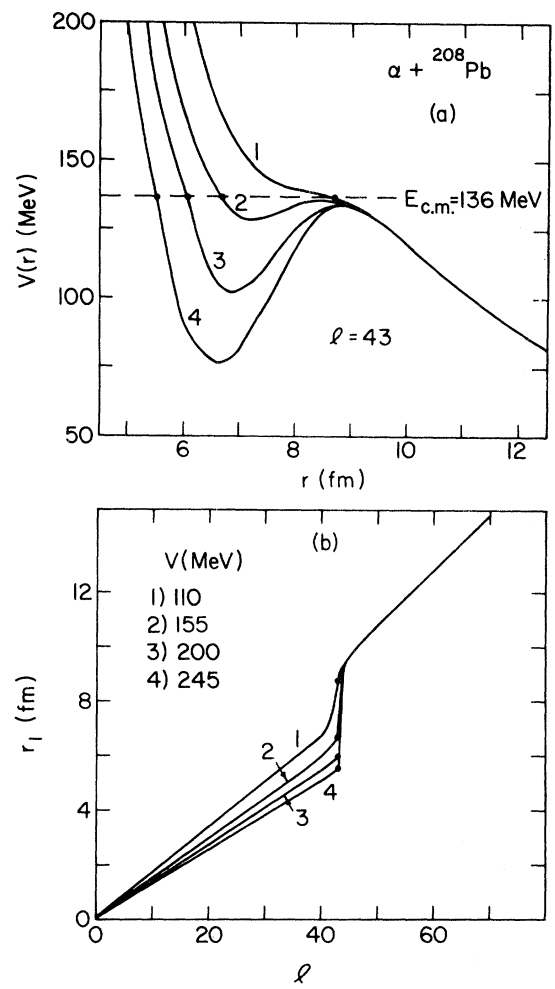

FIG. 9. (a) ^{208}Pb effective potentials for $l=43$ for the different optical potentials listed in Table I which comprise the discrete ambiguity; (b) classical turning points as a function of l value for the same potentials.

approximately π.

It is this abrupt change, occurring here at $l=43$, which allows the different potentials to form the phase ambiguity. The origin of this abrupt change may be seen by considering the l dependence of the effective potential, $V_{\text{eff}}(l,r)=U(r)+V_c(r)+\hbar^2 l(l+1)/2mr^2$. Figure 8 shows the $V_{\text{eff}}(l,r)$ for ^{208}Pb corresponding to potential 1 for several l values in the neighborhood of $l=43$. One sees that as l decreases in the vicinity of $l=43$, the classically defined turning point[17] moves abruptly inward from a point in the far nuclear surface to one well within the nuclear surface. It is this sudden inward movement of the turning point with l that produces the abrupt change in the phase shifts.

The relation between this effect and the discrete ambiguity may be seen by comparing the behavior of the various potentials comprising the ambiguity. Figure 9 shows the variation of turning point with l, along with the effective potentials for $l=43$, for the four potentials in Table I. We observe that the shift in the turning point occurs at the same l value for each of the potentials of the discrete ambiguity, that l value being the one for which the phase shifts (see Fig. 7) exhibit their sudden increase. The discrete ambiguity results then from the fact that the inward movement of the turning point for each of these potentials is sufficiently different to produce the successive difference of π in their real phase shifts.

We now show by examining the ^{58}Ni case that the abrupt shift in the turning point, which allows the phase ambiguity, can be eliminated for a given nucleus at sufficiently high energies. The effective potentials for ^{58}Ni for a number of different l values are shown in Fig. 10. We see, as in the ^{208}Pb case, that the attractive nuclear potential has introduced a dip in the effective potentials for the lower partial waves. However, unlike the situation for Pb, the dip disappears at an energy much lower than the incident energy; in the ^{58}Ni case shown the energy is roughly 60 MeV.

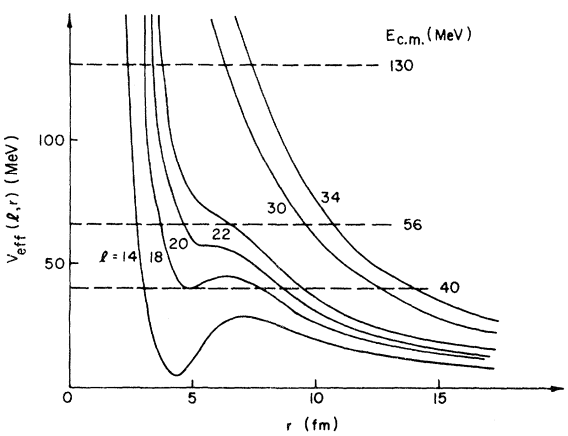

FIG. 10. ^{58}Ni effective potentials for several different l values. The c.m. energies indicated correspond to incident α lab energies of 139, 60, and 43 MeV.

The absence of a dip in the effective potentials for partial waves with turning points well inside the nuclear surface results in the lack of an abrupt change in the turning point as a function of l. The real nuclear phase shifts thus vary smoothly, as seen in Fig. 11(a). We have found that deeper potential wells of the same form are unable to reproduce both this smooth variation and the $n\pi$ increase in the phase shifts for low partial waves, which is necessary for the occurrence of the discrete ambiguity.

At lower energies, however, i.e., at incident energies less than the characteristic energy for the disappearance of the dip, the phase shifts again exhibit the abrupt change as observed for the ^{208}Pb case. The phase ambiguity can then arise. The sudden jump in the phase shifts, present at 43 MeV but absent at 139 MeV, is again related to the corresponding variation of the classical turning points with impact parameter, $(l+\frac{1}{2})/k$, as seen by comparing Figs. 11(a) and 11(b). These results are supported by the inability fo find unambiguous optical potentials for ^{58}Ni at 43,[18,19] 60,[20] and 50 and 64 MeV.[15] We thus conclude that when the incident energy is much greater than the energy characterizing the disappearance of the dip in the effective potentials, multiple phase-shift-equivalent potentials are precluded.

For a given real potential this characteristic energy can readily be calculated. Miller[21] has shown, in a different context, that this energy in the c.m. system is given by

$$\epsilon_{\text{crit}}=[\mathcal{V}(r)+(r/2)d\mathcal{V}/dr]_{\max}, \tag{3}$$

where $\mathcal{V}(r)$ is the sum of the real nuclear plus Coulomb potentials.[22] The value of ϵ_{crit} is primarily determined by the second term in the brackets. Thus, if two nuclei have essentially the same real

TABLE II. The critical energy ϵ_{crit}, as defined in the text, is given below in the lab system for the potentials given in Table I.

Target	V (MeV)	ϵ_{crit} (MeV)
^{58}Ni	116.4	61
^{208}Pb 1	110.0	126
2	155.0	171
3	200.0	225
4	245.0	275

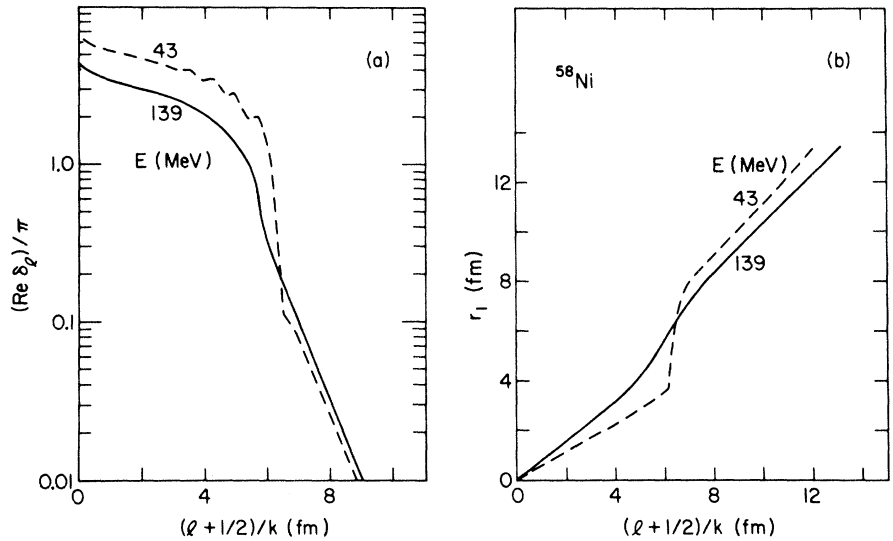

FIG. 11. (a) ^{58}Ni real nuclear phase shifts, and (b) classical turning points as a function of l value. The results are presented for incident energies of 43 and 139 MeV using the ^{58}Ni optical potential of Table I.

nuclear potential except for the radius, $r_0A^{1/3}$, ϵ_{crit} will be larger for the nucleus with the larger radius.

This is demonstrated in Table II where the values for ϵ_{crit} for the potentials of Table I are given. As can be seen, an incident energy of 139 MeV (lab) greatly exceeds ϵ_{crit}(lab) for the ^{58}Ni potential, but only slightly exceeds it for the corresponding ^{208}Pb potential, i.e., potential 1. (This result can be seen graphically by comparing Figs. 8 and 10.) Hence one finds that at this energy it is relatively easy[23] to eliminate the discrete ambiguity in ^{58}Ni, but not so for ^{208}Pb, where at this incident energy, all four potentials produce roughly equivalent phase shifts.

The above comments illustrate the A dependence of the incident energy required to eliminate ambiguities for roughly equivalent potentials. If in fact, the strength of the optical potential increases with A, the A dependence of the required incident energy will be even more pronounced. For example, it need not be inferred that potential 1 is in fact the "true" potential for ^{208}Pb; in fact it appears that potential 2 gives a better fit to the large-angle data than does potential 1. However, regardless of which potential among these in Table I is the "true" one, it is clear that a higher incident energy is required to eliminate ambiguities in the larger ^{208}Pb nucleus than in the smaller ^{58}Ni nucleus.

In a recent elastic scattering investigation[2] on Pb at a higher energy, 166 MeV, only a single potential family was found; it corresponds roughly to potential 1 of Table I. While the incident energy exceeded the ϵ_{crit} calculated from the potential, the angular range of data measured was roughly one-half the value of the calculated maximum deflection angle ($\Theta \approx 100°$). This result is inconsistent with the criteria of Ref. 9, which were stated earlier. A possible explanation of this seeming contradiction may lie in the difficulties associated with fitting differential cross-section data characterized by extremely narrow diffraction oscillations: Small angular errors may produce large errors in the measured cross section; moreover, cross-section maxima and minima tend to be washed out as a result of the finite angular resolution of the detectors. (An opening angle of 0.25° was employed in the present experiment compared to 0.7° in Ref. 2.) The lack of evidence in the data of Ref. 2 for the predicted diffraction structure and the relatively large values obtained for χ^2/F suggest that perhaps such effects were present and that this precluded the finding of other potential families.

IV. INELASTIC TRANSITIONS

A. DWBA Analysis

Differential cross sections were measured for the transitions to 1.45-MeV ($J^\pi = 2^+$), 2.46-MeV (4^+), and 4.47-MeV (3^-) levels in ^{58}Ni, and the 2.62-MeV (3^-) level in ^{208}Pb; they are displayed in Figs. 12 and 13. The excitation energies and spins and parities of these levels are well known from many previous investigations.[24] The data for

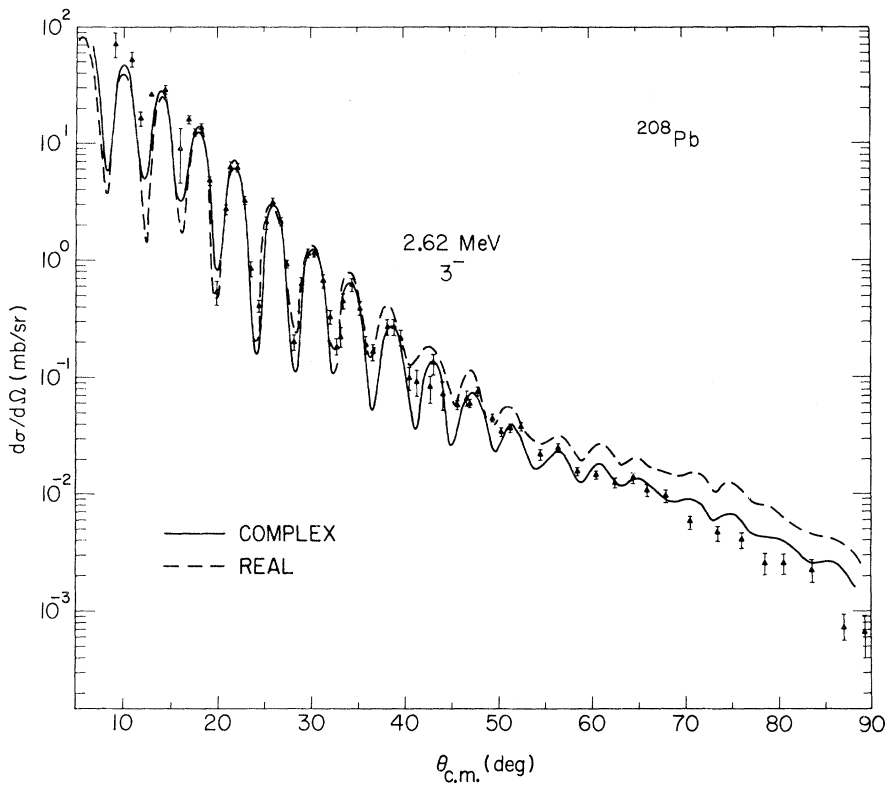

FIG. 12. Differential cross section for the 2.62-MeV ($J^\pi = 3^-$) level of ^{208}Pb. The solid curve was obtained with DWBA calculations utilizing a complex form factor (see text), while the dashed curve results from employing only the real part of the form factor.

the 2^+ and 3^- states obey the Blair phase rule[25] fairly well; the phase of the cross section for the 4^+ level in ^{58}Ni, however, is between that for the 2^+ and 3^- levels. The structure of these states with the possible exception of the 4^+ state in ^{58}Ni, can be generally described within the collective model as one-phonon vibrational states.

We have analyzed the data for these levels with DWBA calculations appropriate for vibrational or rotational excitations. This type of analysis for (α, α') reactions was discussed in detail by Bassel *et al.*,[26] Rost,[27] and Bernstein.[28] Within this formalism the reduced matrix element for an inelastic transition can be written as

$$\langle J_f = l \| V_l \| J_i = 0 \rangle = i^l (2l+1)^{-1/2} \beta_l R_\alpha F_l(r) , \quad (4)$$

where the deformation length $\beta_l R_\alpha$ is related to the amplitude of the radial oscillations of the α optical potential. The radial form factor $F_l(r)$ for direct one-phonon transitions is given by

$$F_l(r) = \frac{V}{a} \frac{d}{dx} [f(x)] + i \frac{W}{a'} \frac{d}{dx'} [f(x')] + F_l^c(r) , \quad (5)$$

where $F_l^c(r)$ is the form factor for Coulomb excitation:

$$F_l^c(r) = \frac{3zZe^2(R_c)^l}{(2l+1)^{2/3} r^{l+1}} (r_0 A^{1/3}) . \quad (6)$$

The other quantities were previously defined (see Sec. III). It should be noted that we have assumed in this formulation that the deformation lengths, $\beta_l R_\alpha$, and not the deformations, β_l, of the real and imaginary parts of the optical potential are equal. This is believed to be a more appropriate assumption for potentials with different real and imaginary geometrical parameters.[28]

The shapes of the theoretical cross sections are completely specified within this model by the parametrization of the optical potential and the angular momentum transfer l. The nuclear structure information is obtained from the value of $(\beta_l R_\alpha)^2$ extracted from normalizing the DWBA angular distributions to the experimental cross sections

$$\frac{(d\sigma/d\Omega)_{\text{exp}}}{\sigma_l(\theta)} = \frac{(2J_f+1)(\beta_l R_\alpha)^2}{(2J_i+1)(2l+1)} , \quad (7)$$

where the quantity $\sigma_l(\theta)$ is numerically calculated with a DWBA computer code. The calculations

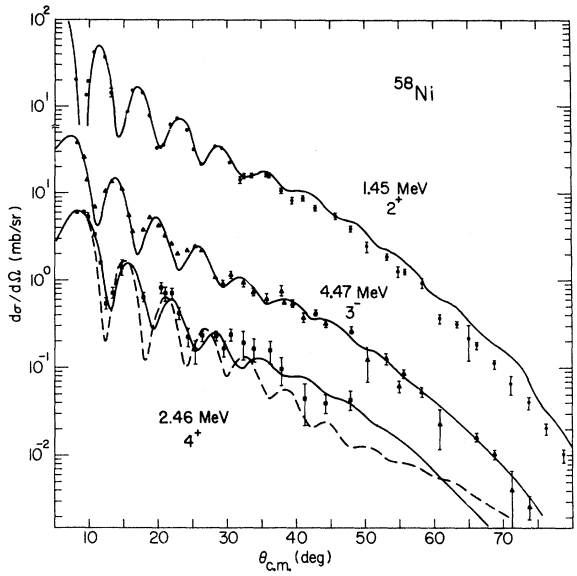

FIG. 13. Differential cross sections for the inelastic transitions to observed levels in ^{58}Ni. The curves are the results of DWBA calculations (see text). The solid curves were obtained with collective-model form factors of a complex first derivative form appropriate for one-phonon excitations; the dashed curve for the 2.46-MeV level was obtained with a second derivative form factor appropriate for a direct two-phonon excitation.

employed in the present analysis were performed with the code TANIA,[29] modified to permit the use of up to 100 partial waves in entrance and exit channels.

The theoretical curves shown in Figs. 12 and 13 are the results obtained with the complex form factors specified above; the predictions agree with the data fairly well. We found a less satisfactory agreement when we employed only the real part of the form factor in the calculations; this is illustrated for ^{208}Pb in Fig. 12. In calculations using only the real part of the form factor the fall-off of the predicted cross section tends not to be as rapid as that of the data. These results appear to indicate the need in this model to employ complex form factors in the α scattering calculations in which the geometrical parameters of the real and imaginary optical potential are different. Similar results have been observed for lower-energy α[18] and ^{3}He inelastic scattering.[30]

In Fig. 13 we present for the 4$^+$ state both the predicted cross section assuming a direct hexadecapole one-phonon transition and that obtained utilizing the direct (single-step, second order in the deformation) part of the two-phonon excitation. The form factor[31] for the latter type of transition is proportional to the second derivative of the optical potential with respect to r. The two-phonon transition strength is thus proportional to $(\beta_2 R_\alpha)^4$, while the one-phonon strength is proportional to $(\beta_4 R_\alpha)^2$.

In several previous inelastic scattering investigations in which the 2.46-MeV level was assumed to be a pure two-phonon state, it was found that calculations employing only direct excitation terms could not adequately describe the data.[18] Buck[31] demonstrated that if one includes multiple excitation terms in addition to these direct terms in a coupled-channels calculation, one can describe the 4$^+$ cross section produced by 43-MeV α particles. Tamura[32] found that by additionally including direct one-phonon excitation contributions in coupled-channels calculations he could successfully describe the differential cross sections for the ground state, 2$^+$ and 4$^+$ states of ^{62}Ni at incident α energies of 33, 50, and 100 MeV.

We find that at an incident α energy of 139 MeV the 4$^+$ differential cross section is adequately described by calculations assuming only a direct hexadecapole one-phonon excitation, that is, calculations employing the first derivative form factor given in Eq. (5). The shape of the cross section is less satisfactorily described by the results

TABLE III. Deformation lengths and transition rates for excited states. Listed for the observed inelastic transitions in each target are the spin and parity of the level, the deformation lengths $\beta_l R_\alpha$ extracted from the present experiment, the range of $\beta_l R_\alpha$ values obtained in previous experiments with α and other projectiles, the isoscalar transition rates assuming a Fermi mass distribution (see text), and the electromagnetic transition rates. The errors in the present values of $\beta_l R_\alpha$ are estimated to be ±10%.

Target	E_x (MeV)	$J^\pi{}_f$	$\beta_l R_\alpha$ present	$\beta_l R_\alpha$ previous [a]	G_l (IS)	G_l (EM) [a]
^{58}Ni	1.45	2$^+$	0.90	0.90-1.07	12.7	10 ±1.5
	2.46	4$^+$	0.30	0.41-0.53 [b]	2.0	...
	4.47	3$^-$	0.68	0.73-0.89	9.2	13 ±2
^{208}Pb	2.62	3$^-$	0.84	0.84	37.1	39.5±2.2

[a] As summarized in Ref. 28 except as noted.
[b] O. N. Jarvis, B. G. Harvey, D. L. Hendrie, and J. Mahoney, Nucl. Phys. A102, 625 (1967).

obtained with a second derivative form factor appropriate for the direct part of a two-phonon excitation. We have not performed calculations to determine the importance of multiple excitation processes.

B. Deformation Lengths and Transition Strengths

In Table III the values extracted for the deformation lengths $\beta_l R_\alpha$ are listed and compared with previous results. The present values agree within the errors with previous measurements. We did not attempt to extract values of β_l alone, since the choice of R_α is nuclear when the real and imaginary radius parameters of the optical potentials differ. For the 3^- state of ^{208}Pb DWBA calculations were performed using each of the various potentials listed in Table I. The shapes and magnitudes of the differential cross sections so obtained did not differ significantly from one another and hence only a single value for $\beta_l R_\alpha$ is quoted.

We also display in Table III the isoscalar transition rates discussed by Bernstein.[28] In much the same way that one can relate electromagnetic (EM) transition rates to oscillations of the nuclear charge distribution, Bernstein defined isoscalar (IS) transition rates which are related to the amplitudes of the oscillations of the nuclear mass distribution. In terms of Weisskopf units the isoscalar transition rates are given by

$$G_l(\mathrm{IS}) = \frac{Z^2(3+l)^2}{4\pi(2l+1)}\beta_m{}^2 c_l\,, \tag{8}$$

where $\beta_m{}^2 = (\beta_l R_\alpha)^2/R_m{}^2$. The quantity $\beta_m R_m$ is the deformation length of the mass distribution and is set equal to that of the optical potential. In the present analysis we employed the conventional choice of $R_m = 1.2A^{1/3}$. To place the IS transition rates on an equal basis with the defined EM rates, the transition rates for a uniform mass distribution must be adjusted to values appropriate for a Fermi distribution. The present experimental values have been adjusted using the factors c_l given by Bernstein.[28] These IS rates are compared with previously measured EM transition rates in Table III. The results are consistent with previous measurements for ^{58}Ni and ^{208}Pb.

V. SUMMARY AND CONCLUSIONS

In our investigation of the elastic and inelastic scattering of 139-MeV α particles from ^{58}Ni and ^{208}Pb, we have been able to resolve the discrete ambiguity in the optical potential for ^{58}Ni, but not for ^{208}Pb. Criteria have recently been developed,[9] based on and illustrated by the present ^{58}Ni data, for the incident energy and angular range of data required to resolve the discrete ambiguity in optical potentials. The comparison of the ^{58}Ni and ^{208}Pb results in the present work illustrates the A dependence of the required incident energy.

This A dependence has been studied further by examining the phase shifts and classical turning points of the real effective optical potentials, $V_{\mathrm{eff}}(l,r)$, for ^{58}Ni and ^{208}Pb. We have given a qualitative explanation of the origin of the phase-shift equivalence of potentials comprising the discrete ambiguity, and have shown further that the minimum energy necessary to eliminate this equivalence can be characterized by the "triple-point" energy ϵ_{crit} of $V_{\mathrm{eff}}(l,r)$. As indicated in Ref. 9, this is also in semiclassical terms, the minimum energy necessary to prevent "spiral scattering."

For potentials with roughly equivalent shapes, the "triple-point" energy of $V_{\mathrm{eff}}(l,r)$ increases with increasing nuclear size. Thus, if one can resolve the discrete ambiguity for a nucleus of a given A at some incident energy, one expects to be able to resolve it at the same incident energy for all nuclei of lower A, but not necessarily for higher A. The former conclusion has been confirmed in a recent experiment[33] involving elastic scattering of 139-MeV α particles by ^{12}C; the latter conclusion is sustained by the present ^{208}Pb results.

Some additional comments may be made on the ^{208}Pb results. The fact that the incident energy is only slightly greater than ϵ_{crit} for potential 1 makes it, in the language of Sec. IIIB, relatively difficult to resolve the discrete ambiguity, assuming that potential 1 is the "true" potential. We note, however, that potential 1 gives a distinctly inferior fit to the large-angle data. The failure of this to manifest itself in an appreciably poorer χ^2/F is due not only to the smaller error bars on the forward-angle points, but to the much larger number of such points, such number being necessary to define accurately the highly structured diffraction pattern. It has been observed previously[34] in a similar context that for this reason absolute reliance on χ^2 as a criterion for goodness of fit may be tempered with subjective judgment of the qualitative appearance of the fit. While not choosing to reject potential 1 on these grounds, we feel that there is evidence that in fact one of the deeper potentials, e.g., potential 2, is the "true" one. If potential 1 is not the "true" one, a rather pronounced A dependence of the strength of the optical potential is indicated in terms of either well depths or volume integrals.

A final point of interest in the elastic scattering results concerns the relation of the optical potentials of composite particles with those of single nucleons. It is commonly suggested that the "true" α optical potential at an incident energy E has a

well depth roughly four times the proton potential well depth for an incident energy $E/4$. The present unambiguous results for ^{58}Ni do not obey this prescription. This relation is also contradicted if one chooses to compare the volume integral per target-projectile nucleon pair; J/M_pM_T for 139-MeV α particles appears to be about $\frac{3}{4}$ of, rather than equal to, that for 30–40-MeV protons. Further investigation of this question is clearly warranted.

The inelastic scattering data do not lead to any unexpected results. The oscillatory portions of the differential cross sections obey the Blair phase rule. The deformation parameters we obtained are in agreement with those determined at lower energies. We also observed that, as with the lower-energy results, optical-model families yielding equivalent fits to the elastic scattering data also give equivalent fits to the inelastic scattering data. An interesting feature of the inelastic scattering results for ^{58}Ni is the similarity of the cross sections at larger angles to those for elastic scattering, in particular the appearance in both of the exponential-like falloff. This result is consistent with the description of elastic and inelastic scattering in the adiabatic approximation given by Austern and Blair.[35] They have explained in detail the observed connection at lower α-particle energies between the diffraction dominated elastic and inelastic scattering. The present results seem to indicate that similar correlations hold beyond the diffraction region.

VI. ACKNOWLEDGMENTS

It is a pleasure to acknowledge our indebtedness to N. R. Yoder for writing the data acquisition code GELIAN, and also for his assistance in expediting the computation procedures used in analyzing the data. We would also like to thank R. A. J. Riddle, H. D. Holmgren, A. A. Cowley, and P. Frisbee for assistance in taking the data. We would also like to express our thanks to the entire staff of the University of Maryland cyclotron.

---

†Research supported in part by the U. S. Atomic Energy Commission.

[1]G. Hauser, R. Löhken, H. Rebel, G. Schatz, G. W. Schweimer, and J. Specht, Nucl. Phys. A128, 81 (1969); J. Specht, G. W. Schweimer, H. Rebel, G. Schatz, R. Löhken, and G. Hauser, *ibid.* A171, 65 (1971), and references therein.

[2]J. Brissaud, M. K. Brussel, M. Sowinski, and B. Tatischeff, Phys. Letters 30B, 325 (1969); B. Tatischeff and I. Brissaud, Nucl. Phys. A155, 89 (1970).

[3]R. Stock, R. Bock, P. David, H. H. Duhm, and T. Tamura, Nucl. Phys. A104, 136 (1967).

[4]R. M. Drisko, G. R. Satchler, and R. H. Bassel, Phys. Letters 5, 347 (1963).

[5]B. Fernandez and J. S. Blair, Phys. Rev. C 1, 523 (1970); J. S. Lilley, *ibid.* 3, 2229 (1971), and references therein.

[6]H. H. Duhm, Nucl. Phys. A118, 563 (1968).

[7]D. A. Goldberg, H. G. Pugh, P. G. Roos, and S. M. Smith, Bull. Am. Phys. Soc. 16, 1284 (1971).

[8]S. M. Smith and D. A. Goldberg, Bull. Am. Phys. Soc. 17, 591 (1972); and to be published.

[9]D. A. Goldberg and S. M. Smith, Phys. Rev. Letters 29, 500 (1972).

[10]B. M. Bardin and M. E. Rickey, Rev. Sci. Instr. 35, 902 (1964).

[11]Isotope Sales Department, Oak Ridge National Laboratory, Oak Ridge, Tennessee.

[12]D. F. Measday and R. J. Schneider, Nucl. Instr. Methods 42, 26 (1966).

[13]F. Perey, private communication.

[14]Such curves tend to be piecewise smooth, only exhibiting abrupt changes in the transition region between "families" (see text later).

[15]D. C. Weisser, J. S. Lilley, R. K. Hobbie, and G. W. Greenlees, Phys. Rev. C 2, 544 (1970), and references therein.

[16]Despite this result that the volume integral rather than V is approximately constant for a given family, the designation of families by V is more widely employed.

[17]At the turning point r_1, $V_{\text{eff}}(l, r_1) = E_{\text{c.m.}}$.

[18]H. W. Broek, J. L. Yntema, B. Buck, and G. R. Satchler, Nucl. Phys. 64, 259 (1965).

[19]D. F. Jackson and C. G. Morgan, Phys. Rev. 175, 1402 (1968).

[20]P. P. Singh, W. T. Sloan, D. W. Devins, and P. Shapiro, Bull. Am. Phys. Soc. 16, 99 (1971).

[21]W. H. Miller, J. Chem. Phys. 51, 3631 (1969).

[22]As discussed in Ref. 9, Eq. (3) in fact gives the minimum energy required to prevent classical "spiral scattering," i.e., to reduce the maximum deflection angle Θ to less than 180°.

[23]According to Ref. 9, the angular range of the data required at incident energies only slightly above ϵ_{crit} is nearly 180°; hence, a large number of data points with relatively small cross sections are required. As the incident energy is raised, however, Θ decreases while the cross section in the region of Θ generally does not (in the case of ^{58}Ni it in fact increases more than tenfold when the incident energy is increased from 60 to 139 MeV).

[24]S. Raman, Nucl. Data B3 (Nos. 3,4), 145 (1970); M. B. Lewis, *ibid.* B5, 243 (1971).

[25]J. S. Blair, Phys. Rev. 115, 928 (1959).

[26]R. H. Bassel, G. R. Satchler, R. M. Drisko, and E. Rost, Phys. Rev. 128, 2693 (1962).

[27]E. Rost, Phys. Rev. 128, 2708 (1962).

[28]A. M. Bernstein, Advan. Nucl. Phys. 3, 325 (1969).

[29]T. Provost and S. M. Smith, private communication.

[30]E. R. Flynn and R. H. Bassel, Phys. Rev. Letters 15, 168 (1965).

[31]B. Buck, Phys. Rev. 127, 940 (1962).

[32]T. Tamura, Progr. Theoret. Phys. Suppl. 37 and 38, 383 (1966).

[33]G. Tibell, A. Cowley, D. A. Goldberg, H. G. Pugh, W. Reichart, S. M. Smith, and N. S. Wall, Bull. Am. Phys. Soc. 17, 465 (1972); S. M. Smith *et al.*, Nucl. Phys. (to be published).

[34]L. N. Blumberg, E. E. Gross, A. van der Woude, A. Zucker, and R. H. Bassel, Phys. Rev. 147, 812 (1966).

[35]N. Austern and J. S. Blair, Ann. Phys. (N.Y.) 33, 15 (1965).

PHYSICAL REVIEW C VOLUME 7, NUMBER 5 MAY 1973

Nuclear Deformation of ^{28}Si from ^{16}O + ^{28}Si Elastic and Inelastic Scattering*

D. S. Gale† and J. S. Eck

Department of Physics, Kansas State University, Manhattan, Kansas 66506

(Received 21 July 1972)

Differential scattering cross sections for the elastic and first excited state inelastic scattering of ^{16}O and ^{18}O from ^{28}Si have been measured at ^{16}O laboratory bombarding energy of 33, 36, and 38 MeV and at an ^{18}O bombarding energy of 36 MeV. The experimental results have been analyzed in terms of coupled channels on the basis of a rotational model. For ^{16}O projectiles the deformation of ^{28}Si was found by this technique to be $\beta_2 = -0.30 \pm 0.08$ and $\beta_4 \geq +0.1$. The cross sections for the scattering of ^{18}O by ^{28}Si could not be described with the deformation parameters obtained from the ^{16}O + ^{28}Si scattering data. The present results are compared with recent experiments using different projectiles and with the results of recent theoretical calculations.

I. INTRODUCTION

It is generally recognized that the first half of the $2s$-$1d$ shell exhibits rotational behavior and is a region of ground-state deformation.[1-10] Recent nuclear structure calculations of the deformation parameters for nuclei in the $2s$-$1d$ shell have stimulated interest in the measurement of these parameters.[11-17] Such data are a critical test of these microscopic calculations. As early as 1957 it was suggested that ^{28}Si has a static oblate deformation.[18] Until recently, however, firm evidence was not available that this region of the s-d shell exhibits a static oblate deformation.[19]

In this paper we describe attempts to measure the deformation of ^{28}Si by coupled-channel analysis of the elastic and inelastic scattering cross sections of ^{16}O + ^{28}Si and ^{18}O + ^{28}Si at energies just above the Coulomb barrier. The main purpose of the present work is to investigate the deformation parameters β_2 and β_4 as a function of the incident particle energy and as a function of various incident particles. It has been previously shown that heavy-ion scattering just above the Coulomb barrier is dominated by surface interactions and therefore provides an excellent method for determining nuclear shapes.[20,21] The use of heavy projectiles such as ^{16}O in this energy range results in a wavelength of relative motion between target and projectile which is smaller than the nuclear surface distortions. The nuclear deformation parameters β_2 and β_4 obtained for ^{28}Si in the present work are compared to recent results obtained using other projectiles.[19,22-27]

II. EXPERIMENTAL PROCEDURE

In this work the elastic and first excited state inelastic differential scattering cross sections for the scattering of ^{16}O and ^{18}O by ^{28}Si were measured. The ^{16}O and ^{18}O beams used in these experiments were obtained from the Kansas State University Model EN tandem Van de Graaff accelerator. Beam energies from 27 to 40 MeV were used. The targets were self-supporting SiO_2 (99.58% enriched ^{28}Si). Target thickness varied from 70 to 120 μg/cm^2. The beam was triply collimated before entering a precision scattering chamber. The diameter of the beam spot on the target was less than 2 mm. Surface barrier detectors with sensitive depths of approximately 100 μm were used to detect the scattered particles. The detectors were mounted on movable arms and collimated so that in all cases they subtended less than 0.5° in the horizontal plane as viewed from the target.

Although kinematic coincidence between the scattered ^{16}O and the recoiling ^{28}Si was tried, this method was not found to be useful, since the multiple scattering of ^{28}Si in the target required that the ^{28}Si detector subtend a large solid angle to insure that all recoil particles were detected. The data reported in this work were obtained from singles spectra. Impurity peaks in the spectra resulting from various ^{16}O + ^{12}C reactions were eliminated by using self-supporting ^{28}Si targets, an oil free vacuum system, and detectors which were too thin to completely stop the resulting α particles. A typical singles scattering spectrum is shown in Fig. 1.